An approach for Robot-Assisted Biosensing: Demonstration with MRI-guided MR Spectroscopy

Ahmet E. Sonmez, *Member, IEEE*, Yousef Hedayati, *Member, IEEE*, Andrew G. Webb, Zhigang Deng, Nikolaos V. Tsekos

***Abstract*— Emerging and established methods, such as optical imaging and MR spectroscopy (MRS), offer new opportunities for *in situ* biosensing. The limited tissue penetration of these modalities can be addressed by locally placing the sensor via minimally invasive trans-needle or trans-catheter access. This work introduces a generic system that mechanically scans an area of interest with a sensor, capable of generating 1D scans while registering them to a guiding modality. Computer simulations illustrate the operation of this approach for a miniature RF coil as the mechanically scanned biosensor. Experimental studies demonstrated the approach on phantoms, using MRI as the guiding modality, and an MR-compatible manipulator, which carried a miniature RF coil, was used to scan and collect MRS and generated 1D MRS scans co-registered to the guiding MRI.**

I. Introduction

New developments in the *in vivo* assessment of molecular and cellular features of lesions, combined with the emergence of molecular/cellular imaging and spectroscopy, offer novel opportunities in basic research and clinical diagnostics, such as the possibility of assessing malignancy of a tumor *in situ* [1, 2]. It is also well recognized that, in several clinical paradigms, multimodal approaches are more appropriate for collection of complementary diagnostic information (e.g., in the case of breast cancer [3-5]).

Molecular and cellular level modalities such as confocal microscopy (COM), optical coherence tomography (OCT) and light induced fluorescence (LIF) have limited tissue penetration (~ 2 mm) [6]. Likewise, spectroscopic methods, such as MR spectroscopy (MRS), suffer from low sensitivity especially at lower field strength scanners and/or when the spectra are collected from a small volume of tissue. Herein, we will refer to those modalities as the "Limited field-of-view" (Lim-FOV).

To address the issue of tissue penetration, endoscopic trans-catheter or trans-needle approaches have been introduced. Likewise for MRS, miniature radiofrequency (RF) coils are used for endoluminal access [7, 8]. These techniques position the sensor inside or in the proximity of the area of interest. The use of Lim-FOV sensors introduces a practical consequence: the placement of the Lim-FOV sensor requires another imaging modality that has sufficient tissue penetration to guide and validate the placement of the former. Demonstrations of this approach include using an ultrasound probe to guide OCT [2] and fluoroscopy to guide intravascular ultrasound [9, 10]. In this work, the imaging modality used to register the Lim-FOV sensor will be referred to as a "Wide-FOV" modality.

Motivated by the merit of combining multiple Lim-FOV sensors that can interrogate the tissue at different levels to provide complementary information about tissue pathophysiology, an approach that uses basic robotic principles to scan and co-register multi-modal-data was developed. Specifically, an actuated manipulator carries the Lim-FOV sensor and scans the tissue via a trans-needle approach. The manipulator is initially registered to the Wide-FOV modality (the Wide-FOV is also used for scouting the area of interest to determine the positions for the manipulator to investigate). The result is the co-registration of the Lim-FOV to the Wide-FOV.

In this work we selected conventional MRI as the Wide-FOV and proton MRS as the Lim-FOV. Cross voxel overlap, while scanning with miniature RF coil is investigated with computer simulations. Then an MR-compatible actuator was obtained and outfitted to carry and spatially scan via trans-needle access, thereby generating one-dimensional (1D) MR spectra (herein referred to as 1D-Scans).

II. Methodology

A. Method and Simulations

Fig. 1(a) illustrates the concept of the proposed method. The manipulator translates the Lim-FOV sensor inside the cannula and stops at preplanned positions Z_J ($1 \le J \le N_{ACQ}$; where N_{ACQ} is the number of acquisition steps). At each Z_J it collects a spectrum V_J. If the positions Z_J are known, then a 1D-Scan of the sensor data can be generated (as shown in Fig. 1(b)). Since in this work, the Wide-FOV modality is

Manuscript received July 3, 2010. This work was supported by the National Science Foundation (NSF) award CNS-0932272. All opinions, findings, conclusions or recommendations expressed in this work are those of the authors and do not necessarily reflect the views of our sponsors.

Nikolaos V. Tsekos is with the Medical Robotics Laboratory, Department of Computer Science at University of Houston, Houston, TX 77204 USA (phone: 713-743-3350; fax: 713-743-3335; e-mail: ntsekos@cs.uh.edu).

Ahmet E. Sonmez and Yousef Hedayati with the Medical Robotics Laboratory, Department of Computer Science at University of Houston, Houston, TX 77204 USA (e-mail: asonmez@uh.edu, yshedayati@uh.edu).

Zhigang Deng and Nikhil Navkar are with the Computer Graphics and Interactive Media Laboratory, Department of Computer Science at University of Houston, Houston, TX 77204 USA (e-mail: zdeng@cs.uh.edu).

Andrew G.Webb is with the Department of Radiology, Leiden University Medical Centre, Leiden, The Netherlands (e-mail: a.webb@lumc.nl).

978-1-4577-0554-0/11/$26.00 ©2011 IEEE

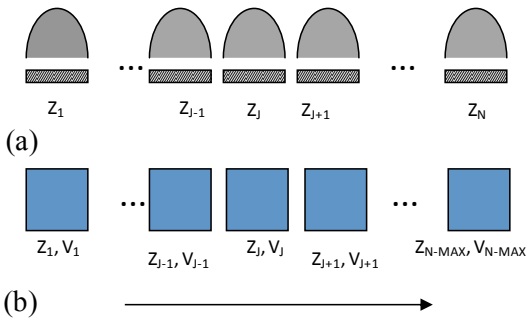

Fig. 1. Graphical illustration of the approach (a) The translating sensor and its sensitive area, (b) 1D-Scan of the sensor data.

MRI, we incorporate a simple registration method: (a) register the initial position of the sensor to the MR scanner's inherent coordinate system (using standard MR methods, discussed in Section 2.C), and (b) calculate the Z_J from the optical encoder signal of the manipulator. Thus the 1D-Scan of the miniature RF coil (Lim-FOV) is registered to the Wide-FOV MRI; the co-registration is achieved by mechanically linking the two modalities via the actuated manipulator.

The described mechanical scanning method exhibits the same fundamental issue with any spatially encoding method: defining the voxel size and shape and determining the associated cross-voxel overlap. Specifically, we simulate the excitation profile of the specific RF coil we used with the Biot-Savart law. The software was developed in-house with MATLAB (Mathworks, Inc., Natick, MA)) to calculate the rotating magnetic field (B1) profile of a four-turn solenoid coil with the dimensions of the one used in the experimental studies (Section 2.B). Fig. 2(a) is a 3D illustration of the coil together with an isosurface that delineates the surface on which the B1 generated by the miniature RF coil is 1% of the maximum B1 (i.e. at the geometric center of the solenoid coil). This figure illustrates the extent of the sensitive area of the coil by the reciprocity principle. It also displays the known features of the coil profile.

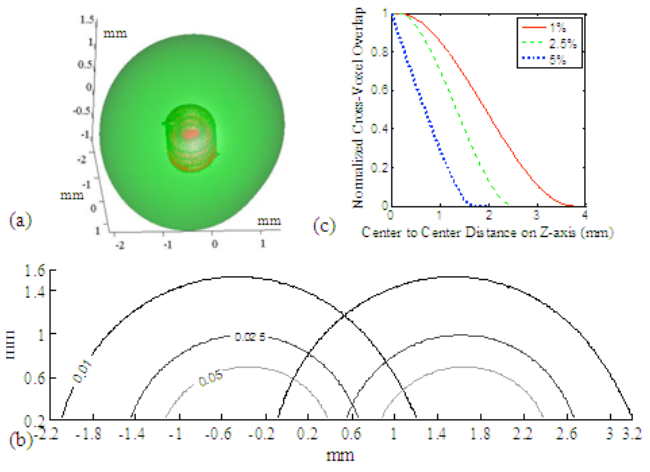

Fig. 2. (a) A surface showing the boundary of one percent signal strength normalized against the total maximum signal strength combined with a simple representation of the simulated coil geometry. (b) Two simulated scanning positions demonstrating the problem of cross-voxel overlap, the contour lines represent 1%, 2.5%, and 5% normalized signal strength respectively. (c) A graph showing the normalized cross-voxel overlap as the distance along the scanning dimension is increased for the 1%, 2.5%, and 5% isosurfaces.

The RF coil reception profile determines the shape and size of the voxel of the MRS sensor. Consequently, the step of motion of the Lim-FOV sensor will also determine potential cross-voxel overlap. This issue becomes relevant when a 1D-Scan of the Lim-FOV is to be overlaid on a Wide-FOV (i.e., which part of the tissue seen on the MR images gives rise to the spectrum collected with the MRS). Obviously, this cross-voxel overlap is reduced as the distance of two consecutive positions of data collection increases. Fig. 2(b) shows two contour plots together, but at different theoretical scanning positions to illustrate the issue of cross-voxel overlap. There are three lines representing each contour with the 1%, 2.5%, and 5% B1 values, again normalized to the maximum B1. Fig. 2(c) shows the percent overlap of two voxels as the center-to-center distance is advanced along the scanning dimension. This cross-voxel overlap calculation helps to plan the spacing between the MRS scans.

B. Hardware

Fig. 3 shows the developed MR compatible manipulator. Its parts were constructed out of non-magnetic and non-conductive acrylonitrile butadiene styrene (ABS). On the distal end is the miniature RF coil (turns = 4, diameter = 1.1 mm and height = 1.2 mm), shown in Fig. 3(a). The coil is connected via a 15 cm long and 1.2 mm diameter semi-rigid coaxial cable (Micro-Coax, Pottstown, PA.) to a balanced-tank circuit for tuning and matching the miniature RF coil to the proton Larmor frequency of 201.5MHz (of the used 4.7 T scanner).

For closed loop control, MR-compatible light-only optical sensors were developed in-house: (a) a linear optical encoder with a resolution of 0.25 mm to encode the translation of the probe and (b) two stop-switches to hard-limit its movement.

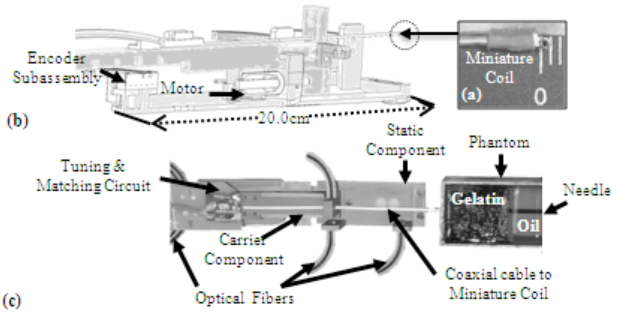

Fig. 3. (a) The miniature 1.1 mm diameter RF coil. (b) Section view of the 3D manipulator design. (c) Top view photograph of the physical prototype of the manipulator and phantom.

The electronics of the sensors were placed at a distance of 7 m from the magnet and were connected to the sensors with optical fibers. The actuator was a piezoelectric Squiggle motor (New Scale Technologies Inc., Victor, NY) connected via a 7 m long shielded cable to its driver and controller. The mechanical and electronic parts were then assembled to the final system (a top side view photograph is shown in Fig. 3(c) at the experimental setup).

C. Experimental Studies

All experimental studies were conducted on a Varian DirectDrive 4.7 Tesla and 21 cm bore MRI scanner (Varian NMR, Palo Alto, CA) spectrometer/imager system, with a 40x45x90 mm^3 rectangular phantom composed of two compartments: one with gelatin, and the other with vegetable oil (Fig. 3(c)). A large volume coil surrounded the phantom (simulating the external coil used in a clinical study) that was used for collecting preliminary images. A registration image was first collected using the miniature RF coil, which appears as a small dot-like marker (~1mm) in the registration image and was used for registering the initial position of the

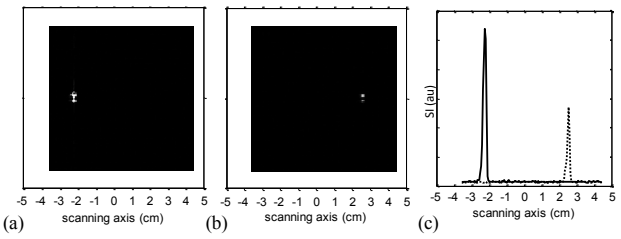

Fig. 4. (a) and (b) MR images collected with the miniature RF coil at the "initial" and "end" position of the scan, respectively. (c) Projections of the SI of the images (a) and (b) along the scanning axis (the difference between the maximum SI of two projections are due the different strength of the MR signals originating from the two compartments).

manipulator (as shown in the Fig. 4). Then, the exact scanning protocol (region, steps and speed of motion) was planned and 1D-Scan MRS was collected by translating the miniature RF coil in steps of 1 mm. After each translation, MR spectrometer is automatically triggered to collect the free induction decay (bandwidth = 5000 Hz and number of points = 2048) after a single excitation pulse (flip angle = 45°). The raw data were Fourier transformed and the 4.79 ppm frequency assigned at the water peak.

III. Experimental Results and Discussion

The device demonstrated MR compatibility without any significant effect on the signal to noise ratio (SNR) of the images, as well as the SNR and linewidth of the spectra. Specifically, with the motor idling, the gradient recalled echo images manifested an SNR for the gelatin compartment of 7.08 ± 0.10 and vegetable oil compartment of 5.72 ± 0.07. When the motor was operating at its set speed, the SNR of the gelatin was 6.79 ± 0.11 and of the oil compartment was 5.62 ± 0.06.

Figs. 5 and 6 show representative results from scanning the two-compartment phantom with the device described herein. The gelatin spectrum, in Fig. 5(a), exhibits a single peak at 4.79 ppm, as a result of the water in the matrix, while the oil, in Fig. 5(b), exhibits multiple resonances from the chemically distinct protons contained in the lipid molecules. Fig 5(c) and 5(d) show contour plots of the spectra with the vertical axis being the axis of scanning. As the sensor crosses the boundary (measured from the Wide-FOV MRI to be at Z = 2 mm) between the two compartments, the water resonance disappears and the oil resonances are observed. This change in spectrum is analogous to the transition between two tissue areas with different MRS properties.

The behavior of the signal along a 1D-Scan and, in particular, at the transition zone between the two compartments can also be appreciated in Fig. 6. It is noted, that the transition zone between the water and the oil compartments is not "sharp"; as shown in Fig. 6(a), the zone is a 4 mm wide void signal (due to susceptibility effects). This void is also reflected into the signal intensity (SI) vs. position graph in Fig. 6(b) that shows a transition band of 2.5 mm (full-width at half-maximum). Another factor contributing to this widened signal-void zone is the expected cross-voxel overlap, shown in Fig. 2(b), since the voxel profile convolves with the actual signal distribution. For the used RF coil and a scanning step of 1 mm between acquisitions, simulations indicate that the cross-voxel overlap is on the order of 86%, 70% and 30%, respectively for 1%, 2.5% and 5% of the maximum B1. Those values are only indicative to the degree of intra-voxel overlapping and specially-designed experimental studies are required in order to quantify and validate it (our work-in-progress). This intra-voxel overlapping, however, affects the reconstruction of the 1D-scan since a spectrum is the integration of signal that may originate from matrix or tissue that give rise to different

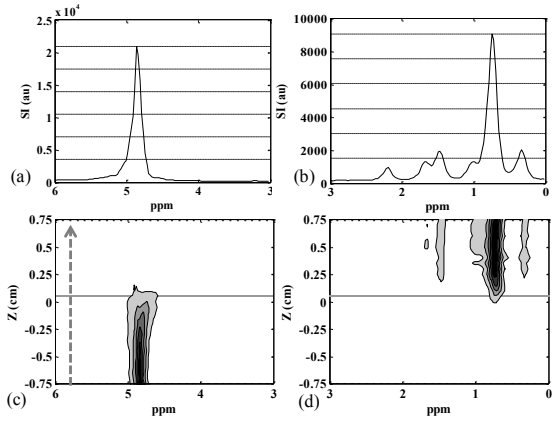

Fig. 5. MRS results from a 1D-Scan. (a) and (b) single spectra from a gelatin and an oil position, (c) and (d) contour plots with the vertical axis being the axis of scanning. Arrow in (c) delineates the direction of scan. The spectra are purposely shown split in two intervals [0-3] ppm, for the oil, and [3-6] ppm, for the gelatin, for better illustration (different signal scales, delineated with the horizontal lines on the corresponding single spectra).

MR signals.

With the described approach, the Wide-FOV and Lim-FOV sensors are "mechanically linked" via the manipulator that is registered to the Wide-FOV modality (i.e. MRI). Therefore, from the forward kinematics of the manipulator, the position of the voxels of the 1D-Scan of the Lim-FOV is known a priori; thus the two modalities are spatially co-registered inherently (i.e. at their genesis). Therefore, this approach enables the direct collection of multi-modal data *in situ* whose co-registration does not need to be calculated algorithmically in post-processing.

In this work for *in situ* scanning, the limited tissue penetration of the Lim-FOV sensors necessitates a trans-needle access. The merits of such minimally invasive access are based on the potential diagnostic information that can be collected. Although established methods currently exist for performing non-invasive single- or multi-voxel MRS with an external RF coil, it is important to emphasize that the miniature RF coil served a purpose that non-invasive alternatives can not address. The results conclude that this miniature RF coil is capable of performing MRS, but more importantly it can be used to register the 1D scan data against the Wide-FOV MRI, which will be critical when a complete sensor array is realized.

The system is designed as an enabling-technology platform that can be adopted to carry and perform scans with other types of sensors. The combination of modalities that interrogate the tissue at different levels, i.e., molecular, cellular and macroscopic, is a unique opportunity in research and potential clinical practice. Current works-in-progress include MR studies to experimentally map the voxel profile generated by the coil, incorporating an MR-compatible sensor for light-induced fluorescence (LIF), developing appropriate code for co-visualization of MRS and LIF, and performing animal studies.

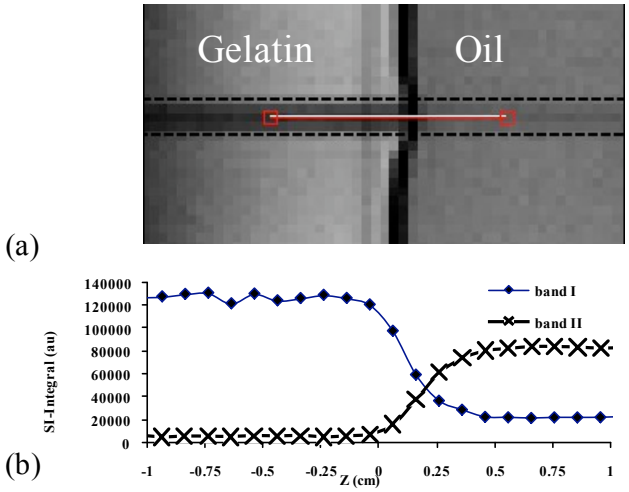

Fig. 6. (a) Zoomed in MRI of the phantom collected with the volume coil, red line is delineating the scanning path and (b) graphs of SI vs. position for bands I = [4.99:4.59] and II = [1.18:0.48].

IV. Conclusions

This paper describes an approach for spatially scanning one or more Lim-FOV sensors with a mechanical manipulator to generate a 1D spatial distribution of the sensor data (i.e., a 1D-Scan of MRS). Using standard robotic methodology, the spatially localized Lim-FOV sensor data are registered relative to the guiding Wide-FOV (i.e., MRI). With the incorporation of other appropriate Lim-FOV sensors (LIF, OCT, COM etc…), this approach can function as the framework to use established Wide-FOV modalities (MRI, ultrasound, etc.) to guide localized assessment of the tissue-specific molecular fingerprints and cellular properties *in situ*.

References

[1] D. J. Margolis, J. M. Hoffman, R. J. Herfkens, R. B. Jeffrey, A. Quon, and S. S. Gambhir, "Molecular imaging techniques in body imaging," *Radiology,* vol. 245, pp. 333-56, Nov 2007.

[2] Q. Zhu, M. Huang, N. Chen, K. Zarfos, B. Jagjivan, M. Kane, P. Hedge, and S. H. Kurtzman, "Ultrasound-guided optical tomographic imaging of malignant and benign breast lesions: initial clinical results of 19 cases," *Neoplasia,* vol. 5, pp. 379-88, Sep-Oct 2003.

[3] S. E. Harms and D. P. Flamig, "Breast MRI," *Clin Imaging,* vol. 25, pp. 227-46., 2001.

[4] A. P. Smith, P. A. Hall, and D. M. Marcello, "Emerging technologies in breast cancer detection," *Radiol Manage,* vol. 26, pp. 16-24; quiz 25-7, Jul-Aug 2004.

[5] C. P. Behrenbruch, K. Marias, P. A. Armitage, M. Yam, N. Moore, R. E. English, J. Clarke, and M. Brady, "Fusion of contrast-enhanced breast MR and mammographic imaging data," *Med Image Anal,* vol. 7, pp. 311-40, Sep 2003.

[6] F. A. Jaffer, C. Vinegoni, M. C. John, E. Aikawa, H. K. Gold, A. V. Finn, V. Ntziachristos, P. Libby, and R. Weissleder, "Real-time catheter molecular sensing of inflammation in proteolytically active atherosclerosis," *Circulation,* vol. 118, pp. 1802-9, Oct 28 2008.

[7] B. Qiu, F. Gao, P. Karmarkar, E. Atalar, and X. Yang, "Intracoronary MR imaging using a 0.014-inch MR imaging-guidewire: toward MRI-guided coronary interventions," *J Magn Reson Imaging,* vol. 28, pp. 515-8, Aug 2008.

[8] H. H. Quick, J. M. Serfaty, H. K. Pannu, R. Genadry, C. J. Yeung, and E. Atalar, "Endourethral MRI," *Magn Reson Med,* vol. 45, pp. 138-46, Jan 2001.

[9] M. Piedra, A. Allroggen, and J. R. Lindner, "Molecular imaging with targeted contrast ultrasound," *Cerebrovasc Dis,* vol. 27 Suppl 2, pp. 66-74, 2009.

[10] I. Springer and M. Dewey, "Comparison of multislice computed tomography with intravascular ultrasound for detection and characterization of coronary artery plaques: a systematic review," *Eur J Radiol,* vol. 71, pp. 275-82, Aug 2009.